Jurnal Kejuruteraan 34(4) 2022: 659-670
https://doi.org/10.17576/jkukm-2022-34(4)-14

12-APR Segmentation and Global Hu-F Descriptor for Human Spine MRI Image Retrieval

W Mimi Diyana W Zaki[a*], Ling Chei Siong[a], Aini Hussain[a], W Siti Halimatul Munirah W Ahmad[b] & Hamzaini Abdul Hamid[c]

[a]Center for Integrated Systems Engineering & Advanced Technologies (INTEGRA), Department of Electrical, Electronic and Systems Engineering, Faculty of Engineering and Built Environment, Universiti Kebangsaan Malaysia, Bangi, 43600, Selangor DE, Malaysia,
[b]Faculty of Engineering, Multimedia University, 63100 Cyberjaya, Malaysia
[c]Universiti Kebangsaan Malaysia Medical Centre, Department of Radiology, Cheras, 56000, Selangor, Malaysia,
Faculty of Engineering & Built Environment, Universiti Kebangsaan Malaysia, Malaysia

**Corresponding author: wmdiyana@ukm.edu.my*

Received 27 May 2021, Received in revised form 28 October 2021
Accepted 28 November 2021, Available online 30 July 2022

ABSTRACT

The image retrieval system has been used to provide the needed correct images to the physicians while the diagnosis and treatment process is being conducted. The earlier image retrieval system was a text-based image retrieval system (TBIRS) that used keywords for the image context and it requires human's help to manually make text annotation on the images. The text annotation process is a laborious task especially when dealing with a huge database and is prone to human errors. To overcome the aforementioned issues, the approach of a content-based image retrieval system (CBIRS) with automatic indexing using visual features such as colour, shape and texture becomes popular. Thus, this study proposes a semi-automated shape segmentation method using a 12-anatomical point representation method of the human spine vertebrae for CBIRS. The 12 points, which are annotated manually on the region of interest (ROI), is followed by automatic ROI extraction. The segmentation method performs excellently, as evidenced by the highest accuracy of 0.9987, specificity of 0.9989, and sensitivity of 0.9913. The features of the segmented ROI are extracted with a novel global Hu-F descriptor that combines a global shape descriptor, a Hu moment invariant, and a Fourier descriptor based on the ANOVA selection approach. The retrieval phase is implemented using 100 MRI data of the human spine for thoracic, lumbar, and sacral bones. The highest obtained precision is 0.9110 using a normalized Manhattan metric for lumbar bones. In a conclusion, a retrieval system to retrieve lumbar bones of the MRI human spine has been successfully developed to help radiologists in diagnosing human spine diseases.

Keywords: Image segmentation; active shape model; feature extraction; image retrieval; human spine; MRI images

INTRODUCTION

Magnetic resonance imaging (MRI) is a non-invasive diagnostic tool that works by applying radio waves and strong magnetic field to produce images. Unlike computed tomography (CT), MRI does not produce radiation and prevents radiation exposure to subjects. Thus, MRI has been widely used to evaluate various spinal diseases, such as disc degeneration and herniated discs (Y.-J. Zhao et al. 2011) and the most frequently used imaging test for brain and spinal cord ("MRI - Mayo Clinic" n.d.). MRI provides details on the structural features of internal body tissues, including spinal disc, nerve, spinal cord, and spinal fluid. However, CT scans are better than MRI scans at examining lung tissues, considering that the latter can be noisy and takes longer to complete than the former. Moreover, studying medical images is time-consuming and subjective depending on the experience of radiologists (F. Zhao & Xie 2013). Thus, by integrating computer processing into spinal MRI, an easy, time-efficient, and more accurate diagnosis can be achieved (Shi et al. 2007).

The human spine comprises 33 connected bones to support body weight and it allows humans to stand upright and bend while protecting the spinal cord from injuries. The 33 connected bones are divided into five parts which are cervical, thoracic, lumbar, sacrum, and coccyx. Each part performs specific function. Spinal fracture is one of the common injuries that may occur to the spinal vertebra due to road accidents, falls, sports, and diseases such as spine tumors and osteoporosis. The vertebra dislocation or fracture can cause bone fragments to pinch and damage the spinal nerves or spinal cord. It is reported in (Tong et al. 2016) that cases of spinal cord damage, especially due to the vertebral fracture of the spine, have increased. The vertebral fracture can occur anywhere along the spine as reported by previous studies such as fractures at the cervical (Groen et al. 2016; Korhonen et al. 2014; Majkowska et al. 2014; Wysham et al. 2017), and lumbar portions (Grierson et al. 2015; Kaufman

et al. 2013). Moreover, there is an increasing interest in the studies on vertebra and disc segmentation using MRI scans reported in the past 10-15 years (Rak & Tönnies 2016) due to the fact that the MRI has become the most suitable medical imaging technique for diagnosing many diseases in the medical discipline given its adoption of non-invasive imaging technology which does not pose harm to human health (Deng et al. 2016).

Medical image segmentation is one of the computer processing parts that plays a crucial role in many imaging applications. The process is conducted by automating or facilitating the delineation of anatomical or bone structures and other regions of interest (ROIs). The image segmentation is important in the feature-based technique implementations for searching image databases. Effective segmentation will isolate important images with homogenous regions in the database, where feature vectors are calculated for searching. A manual segmentation of all database images is an extremely lengthy and tedious process, therefore a fully- or semi-automate segmentation procedure will produce significant gains. Nevertheless, the development of a fully automated segmentation for the human spine is a challenging task because of the low resolution and strong noise presented in the MRI images. Thus, numerous works on segmentation have been proposed to overcome these limitations (Bazila & Mir 2014).

Modern standards such as digital imaging and communications in medicine (DICOM) and picture archiving and communication system (PACS) offer an efficient way to store and transfer the images and improve interoperability. DICOM is the industry standard for the data storage and transmission of digital images as well as other related information among imaging devices. It offers all essential tools for the diagnostically precise medical imaging data representation and processing. DICOM is an all-encompassing data storage, transfer, and display protocol that is built and designed to fulfil all functional parts in digital medical imaging (Pianykh 2008), including a standardized file format. However, as it is only a set of standards, it needs a medical system (i.e. PACS) to ensure interoperability with the functionality of PACS being DICOM-driven. The PACS that is an image retrieval system (IRS) based on texts has been widely used in medical institutions, where it is dedicated to the storage, retrieval, distribution, and presentation of medical images.

The text-based image retrieval (TBIR) uses a textual resource of information to find out an image's subject matter, for instance an annotation or more structured metadata. The TBIR first annotates the image using text and then applies a text-based management system to perform image retrieval. However, this method suffers from two major problems when dealing with a large volume of image collections. First, a vast amount of labor is required in the manual image annotation or indexing. This process is cumbersome, prone to error, and prohibitively expensive. Another problem with manual annotation is subjectivity. For example, a specialist may be interested in only a particular aspect of the image at a certain period of time, therefore, other aspects may not be captured in the annotation. These problems may lead to unrecoverable mismatches in later retrieval process. Thus, these limitations have resulted in the development of a content-based image retrieval (CBIR) system (Sharma et al. 2012).

CBIR uses features solely from the image, such as the shapes, texture, and color to find out its subject matter. CBIR has been developed to offer a solution to the previously mentioned drawbacks of the TBIR system. CBIR refers to the retrieval of images from a database using information obtained from the images themselves, rather than only from associated text indices. The visual features of images are extracted, and then similarities are measured to determine the most similar images from a database (Syam et al. 2013) or to retrieve visually similar diseases (Ahmad et al. 2014). This retrieval system offers radiologists with a diagnostic help in the form of display of related previous cases, along with verified pathology and other appropriate information. Nevertheless, retrieving medical images from a large database may be computationally expensive. Hence, improving visual feature extraction is also necessary to reduce retrieval time (Shrinivasacharya & Sudhamani 2014) while retaining the system's high-precision characteristic. Thus, our research proposes a semi-automated segmentation method using a 12-anatomical point representation. Then, the features of the segmented ROI are presented with a new global Hu-F descriptor for human spine retrieval in MRI images. The retrieval of archived medical images is useful in aiding the diagnosis of and providing evidence from previous cases, as well as in training junior radiologists. Considering that spinal diseases can be represented by specific regions of an image, a retrieval system with accurate features is necessary. This study presents another useful contribution in retrieving similar cases involving thoracic, lumbar, and sacral bones. The following sections are described as follows. Section II introduces related work to this study, followed by Section III that describes the research methodology. Section IV presents the results and performance evaluation, and Section V provides the conclusion and summary.

RELATED WORK

VERTEBRA SEGMENTATION

There are numerous works conducted on the vertebra segmentation of the human spine using MRIs, such as Huang et al. (2009) included a system with fully automatic vertebra detection and segmentation for spinal MRIs. The system proposed a statistical learning approach based on an improved AdaBoost algorithm to detect the vertebra. Then, the method was refined and segmented with an iterative normalized-cut segmentation algorithm. It has successfully achieved nearly 98% vertebra detection and 96% segmentation accuracy relative to active contour and level set segmentation. In addition, Neubert et al. (2011)

developed a system for automated 3D segmentation of vertebral bodies and intervertebral discs from MRIs. The segmentation approach was based on statistical shape analysis and template matching of grey-level intensity profiles.

Egger et al. (2012) proposed a rectangle-based segmentation algorithm in which the method would perform a graph cut to separate the object from the background. Using this approach, problems in the normal graph-based algorithm were solved by referring to the rectangular shape of the object during the sampling graph nodes, and an accuracy of approximately 90% was achieved. On the other hand, Schwarzenberg et al. (2014) developed another graph-based method using a cubic template for volumetric MRI vertebrae segmentation, which was an extension of an earlier work (Egger et al. 2012). With only one click and the running time less than 60s, the proposed algorithm was performed with an average dice similarity coefficient (DCS) of 81.33%. This was easier to conduct as compared to the square cut method.

In another work, Zukić et al. (2012) segmented vertebral bodies in MRI images using multiple-feature boundary classification and mesh inflation. This approach required a manual seed point input, thus rendering it semi-automatic. The algorithm was performed with the accuracy of 78%. Meanwhile, (Ben Ayed et al. 2012) employed convex relaxation and distribution matching method to segment the vertebral body in MRIs. Tested on 13 mid-sagittal 2D MRIs, the proposed method achieved DCS of more than 80%. This approach is suitable for parallel computations and it does not require complex learning from a large training set. An approach for segmenting articulated spine shape models in CT and MRI images using manifold embedding and higher-order Markov random field were introduced by (Kadoury et al. 2013). The approach obtained notably good segmentation results. In another work (Lootus et al. 2014), a histogram of gradient-oriented image descriptors was combined with a graphical model to localize and label the vertebrae in lumbar MRI images. The algorithm was claimed to be simple and computationally cheap procedure, yet was also applicable to CT scans.

FEATURE EXTRACTION

Content-based image retrieval system (CBIRS) uses image as an input, hence the retrieval result relies on the visual characteristics which are color, texture, and shape of an image. Shape, which refers to the geometry details of an object, is one of the most important features of an image. Comparing to other visual features, shape feature is more efficient in differentiating image content as it is easy to be detected by the human eye (Thomas & Sreekumar 2014; Wang et al. 2011). Injuries or diseases of the spine normally result in shape changes, which implies that spine abnormalities can be identified on the basis of vertebral shapes (Barbieri et al. 2015; Hille et al. 2016). Figure 1 shows two examples of fracture, which are a compression fracture and a thoracic fracture that may occur at the vertebras.

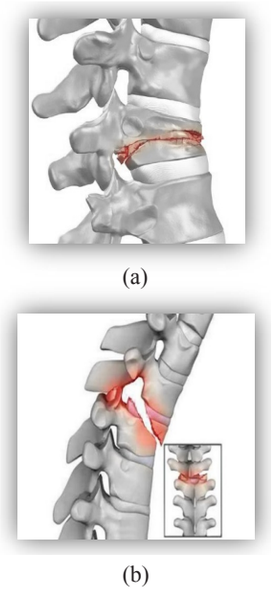

(a)

(b)

FIGURE 1. (a) Compression fracture (Brisson n.d.) and (b) thoracic fracture (Gupta n.d.) of the vertebra

Fourier descriptor (FD) is a powerful feature for boundaries and objects representation, which has been successfully applied in many applications related to shape (Hu & Li 2013; Yasmin et al. 2013). FD was utilized in a previous work (Gang et al. 2012) by combining centroid distance, complex coordinates, and curvature, in which centroid distance derived the best result among the three combinations. FD was also adopted by other studies (Lande et al. 2014; Mary Helta Daisy et al. 2013) in relation to CBIRS.

Hu moment invariants (Hu) is one of the most popular techniques in extracting image features in object recognition and classification (Iqbal et al. 2012). The invariant moments derived by Hu (Ming-Kuei 1962) defined seven moments that enable moment calculations that are invariant under rotation, scale, and translation. This includes the skew invariant that is able to differentiate mirror images of the same images. Hu was used as a shape feature to classify malicious and non-malicious regions in images (Duan et al. 2014), and it was also utilized in pathological brain detection (Zhang et al. 2015).

On the basis of the literature review, FD and Hu were selected in this study together with the global shape descriptor (GSD), and their efficiencies were investigated in medical IRS application.

RESEARCH METHODOLOGY

Figure 2 presents a proposed framework of the medical image retrieval system (MIRS). This study is a continuation of a preliminary work conducted using TBIRS (Ahmad et al. 2018). The proposed retrieval system consists of two stages, which are an offline feature extraction

stage and an online retrieval stage. The MIRS in this work is driven by CBIRS, in which the initial steps include the preprocessing and segmentation phases. These steps are developed to increase image contrast, reduce noise, and extract ROIs from images.

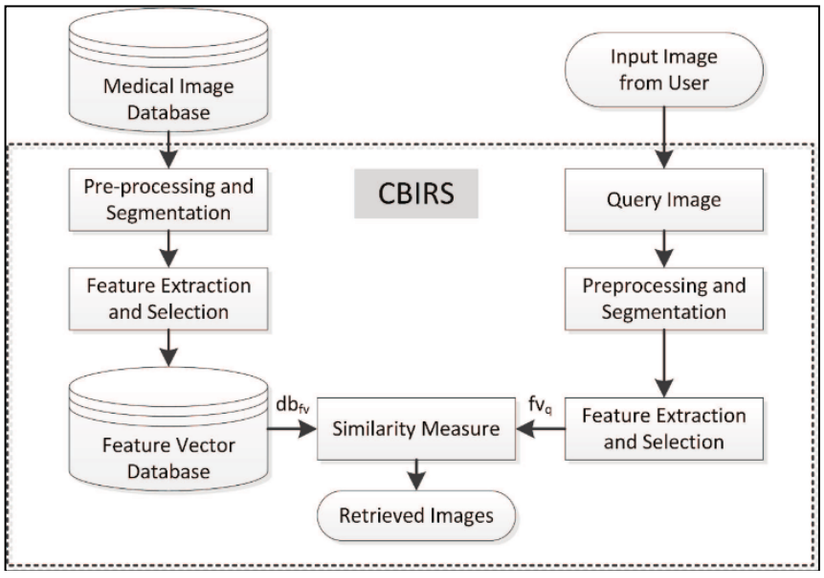

FIGURE 2. MIRS framework driven by CBIRS

The next step involves feature extraction and selection, in which features from an image are extracted and analyzed to select the most suitable features. The selected features are then combined to produce a new feature vector (FV), which is stored in the feature vector database (FVD) to be used by online users. These processes are running during the offline stage. During the online stage to retrieve an image, the user must provide a query image, and query features will be computed and compared with FVs in the FVD based on a similarity measurement; the smaller the measure, the similar the image. Thus, for retrieval, the similarity measurements are sorted in ascending order. Lastly, all similar images related to the query are shown ascendingly in a display panel, i.e. a created result panel of the developed CBIRS.

SEGMENTATION

Segmentation is a necessary phase in the ROI extraction of an image as ROIs are used as the basis of texture, color, or shape features. A fully automated image segmentation into objects is still an unresolved crisis. Even in specialized domains, the fully automated segmentation is often difficult to realize. Under-segmentation, over segmentation, and boundary inaccuracy are among of the problems encountered with image retrieval using the segmentation-based approach. As reported in (Bazila & Mir 2014; Shi et al. 2007; F. Zhao & Xie 2013; Y.-J. Zhao et al. 2011) segmentation-based approaches are used to address locality, in which the spine MRI images are first segmented to identify different bones and then features are subsequently extracted from the segmented bones. Thus, this study proposes a semi-automated segmentation approach, namely, the 12-anatomical point representation (12-APR), to extract the ROIs of the human spine according to thoracic (T), lumbar (L), and sacral (S) bones. The approach is based on active shape models (ASMs), in which the models must be trained using training images (Cootes et al. 1995), and their application has been successful in various medical fields (El-Rewaidy et al. 2018; Wu et al. 2018). In this study, a set of landmark points is used to characterize the vertebral (T, L, and S) contours. Figure 3 presents a graphical summary of the main steps of the proposed 12-APR. In this experimental work, the point annotation process must be delineated with a set of guidelines as illustrated in Figure 4. Landmark points are carefully marked to ensure high accuracy of the constructed shape model. The annotated points serve as the training sample for each image derived by the landmark points.

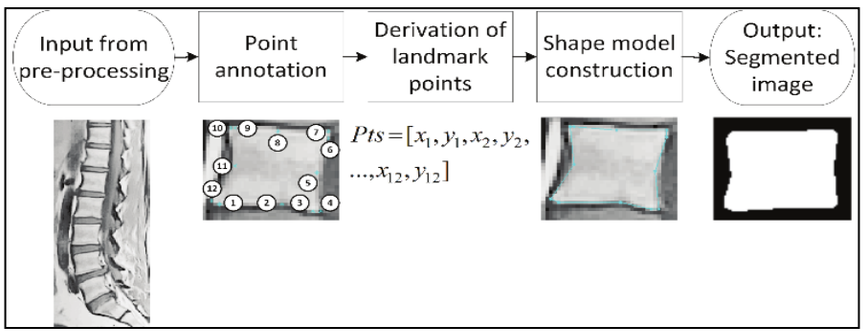

FIGURE 3. Three main steps of the proposed 12-APR approach

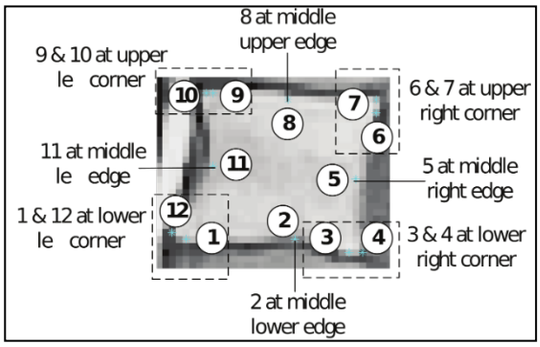

FIGURE 4. Guidelines for the delineation of landmark points of the vertebra

The ASM is constructed based on a collection of training samples, which are collectively represented by a statistical model of the vertebral bone appearance. This model involves two other sub-models which are profile and shape models. The profile model is built for each landmark point based on the points' analyses, learned characteristics in the training stage, and behavior information around the points of the stored image. To match the shape features, the region landmark points in the test image are carefully adjusted to fit the profile model. The shape model represents all tolerable positions of the landmarks, and it ensures that the adjustment of the profile model does not result in a change in the shape's mean values during the matching with the test image. For comparison, the shape model acts on the entire image (global), whereas the profile model acts on individual landmarks (local). Initially, these two models continue correcting and improving one another until the system has no more room for adjustment. Then, regional delineation is performed by collecting the details of information to determine which of the details can finely fit the model after completing the training process. The mean value of the shape feature, which is calculated during the training, and examined profiles are superimposed on the landmark points to match the vertebral shape with the test image. Finally, the delineated test image is converted into a binary image as an ROI. Details on the shape features are explained in the next section.

FEATURE EXTRACTION AND SELECTION

In this work, a new FV known as global Hu-F descriptor is proposed. The features extracted from GSD, Hu, and FD techniques are optimally selected based on analysis using ANOVA, a statistical model that can assess potential differences of the group mean values. This statistical model is used to determine if there are any significant potential differences among the three vertebral bone types that are T, L, and S. The optimal feature vector selected from the three techniques (GSD, Hu, and FD) are stored in the FV database db_{fv} and used in the retrieval phase.

In general, GSD can differentiate large dissimilarities among shapes. However, this fundamental feature type is not suitable as a standalone shape descriptor. In particular, this feature must be combined with other descriptors, such as centroid (C), area (A), bounding box (Bb), perimeter (P), solidity (Sd), equivalent diameter (Eq), extent (Ex), eccentricity (Ecc), major (MaX) and minor axes (MiX), and orientation (O). Some of these features can be illustrated directly in their basic forms, as shown in Figure 5. Meanwhile, other features can be derived from the geometric properties of a region.

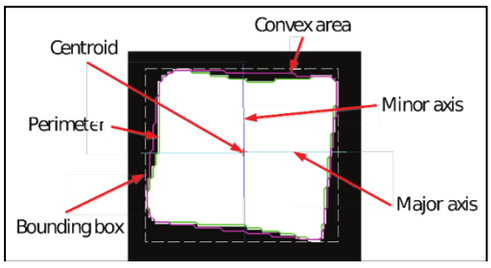

FIGURE 5. Some of the GSD for a region

Hu, which can define seven moments and enable moment calculations that are invariant under translations and changes in scale and rotation is perceived as an innovative work (Ming-Kuei 1962). This model includes a skew invariant that can distinguish the mirror images of otherwise identical images. In addition, the main concept of FD is the use of the Fourier-transformed boundary as the

shape feature. A modified FD, which is robust to noise and invariant to geometric transformations (Rui et al. 1998). Ahmad and Fauzi (2008) also adapted the same approach. that considered an N-point digital boundary starting from an arbitrary point ($x0$, $y0$), followed by a steady counterclockwise movement along the boundary. Then, a set of coordinate pairs, i.e., ($x0$, $y0$), ($x1$, $y1$),..., (x_{N-1}, y_{N-1}), was generated. These coordinates are expressed in a complex form, i.e. $z(n) = x(n) + jy(n)$, $n = 0,1,2,..., N-1$. Equation (1) shows the formulation of discrete Fourier transform (DFT) of $z(n)$ where the complex coefficientis referred as FD of the shape boundary. In this experimental work, 32-point DFT was used, thus resulting a 32-dimensional FV.

$$a(k) = \sum_{n=0}^{N-1} z(n) \exp[\frac{-j2\pi kn}{N}], 0 \le k \le N-1 \quad (1)$$

Retrieval

To perform a retrieval task in CBIRS, a vertebral image (T, L, or S) is selected as a query image, and a query FV denoted fv_q as is computed. Then, similarities between the query image and the database images are calculated by comparing fv_q with all FVs in db_{fv}. This study employs Manhattan (M and Euclidean (E distances, as well as normalized Euclidean (NE) and normalized Manhattan (NM) distances to measure the similarities. The FV normalization may solve the wide range of difference in FV values, leading to insignificant contributions of certain features to the retrieval performance. A smaller distance value implies that the corresponding image is the most similar to the query image and vice versa. Given f^i and f^j as query and retrieved FV at a time, the four-distance metrics are given in Equations (2) to (5).

$$E = \sqrt{\sum_{k=1}^{n} \left(f_k^i - f_k^j\right)^2} \quad (2)$$

$$NE = \sqrt{\sum_{k=1}^{n} \frac{\left(f_k^i - f_k^j\right)^2}{\sigma_k}} \quad (3)$$

$$M = \sum_{k=1}^{n} \left|f_k^i - f_k^j\right| \quad (4)$$

$$NM = \sum_{k=1}^{n} \left|\frac{f_k^i - f_k^j}{\sigma_k}\right| \quad (5)$$

Where σ_k is the standard deviation of the k[th] feature in the FV database (Ahmad & Fauzi 2008).

EVALUATION

In this experimental work, validation process is necessary to quantify the performance of the segmentation method. The most straightforward validation approach is by comparing the segmentation results obtained from a developed segmentation method with a manually ground truth preparation. The choice of the performance measure depends on the application and it can be based on a region's information (number of misclassified pixels) or boundary information (distance to true boundary). In this study, the proposed segmentation method produces binary masks as the final segmentation output. Ground truth data are obtained by manually tracing vertebral bones, as validated by two expert radiologists from the Department of Radiology, Universiti Kebangsaan Malaysia Medical Centre, Malaysia. Consequently, the binary images are compared with the corresponding hand-segmented images according to pixels. Each pixel is classified in one of the four categories: true positive (TP), true negative (TN), false positive (FP), and false negative (FN) as summarized below.

1. TP: area correctly classified as vertebral bone region
2. TN: area correctly classified as background
3. FP: area incorrectly classified as vertebral bone region
4. FN: area incorrectly classified as background

To validate the efficiency of the proposed 12-APR segmentation method, the classical measures of segmentation accuracy (Acc), sensitivity (Se), and specificity (Sp). In addition, other two standard performance indicators, i.e. area under the curve (AUC) for receiver operating characteristics (ROCs) and F-score are also employed. Unlike accuracy, the F-score is independent from the true negative fraction, as defined by Equation (6), in which A and B are the segmented vertebral bone regions or sets of nonzero pixels in the first and second binary masks, respectively. These regions correspond to the ground truth (A) and algorithm-segmented masks (B), while ∩ represents the intersection of the two sets.

$$F = \frac{2|A \cap B|}{|A| + |B|} \quad (6)$$

The feature extraction and selection phase, as well as the retrieval phase, are evaluated according to the standard measure of the information retrieval system which are precision, and recall. Precision rate is defined as the fraction of images of the answer to the query that have been identified as relevant, while recall rate is the fraction of relevant images of the answer to the query. Recall and precision are normally presented on opposing axes on a graph. The graph is constructed by plotting the precision and recall values calculated up to each of the rankings.

RESULT AND DISCUSSION

The experimental results of segmentation, the CBIRS design, and the results of the feature extraction and selection and retrieval phases are discussed in the following sections.

Segmentation Result

The vertebra segmentation was performed on the randomly selected 15 MRI images. This evaluation process was conducted with the help of four observers, i.e. expert radiologists (ER1 and ER2) and non-radiologists (NR1 and NR2). Performance of the proposed semi-automated 12-APR segmentation method was compared between the 9-APR technique (Mustapha et al. 2015) and a manual segmentation by ER1, ER2, NR1, and NR2. For each method, the comparison was done using 15 output images segmented by an observer and 15 corresponding ground truth images. Table 1 lists the summary of the results. The table shows that the outputs of all three methods done by all observers give excellent segmentation results with Acc, Se, Sp, and AUC values ranges between 0.990 to 0.998. Nevertheless, based on the average F-score values of the four observers, the proposed 12-APR outperformed 9-APR and manual segmentation methods.

Figure 6 shows the ROC curve of the segmentation that was analyzed by using logistic regression without cross validation to verify the overall performance of the proposed 12-APR method. The S bone classification obtained the best result with AUC = 1, whereas the L and T bone classifications obtained AUC = 0.9205 and AUC = 0.9213, respectively. The number of images in the database helped derive considerably excellent results. Hence, in future work we are looking forward to testing the algorithm by using additional spine MRI images to evaluate its robustness.

TABLE 1. Summary of the average of segmentation performances by each observer

Metric	METHOD	Observer			
		ER1	ER1	NR1	NR2
Acc	12-APR	0.998	0.997	0.998	0.999
	9-APR	0.998	0.997	0.998	0.998
	Manual	0.997	0.997	0.998	0.998
Se	12-APR	0.998	0.998	0.998	0.990
	9-APR	0.997	0.933	0.994	0.993
	Manual	0.991	0.997	0.978	0.998
Sp	12-APR	0.998	0.997	0.998	0.999
	9-APR	0.998	0.997	0.998	0.998
	Manual	0.997	0.997	0.998	0.998
F	12-APR	0.867	0.845	0.882	0.913
	9-APR	0.856	0.782	0.880	0.893
	Manual	0.845	0.822	0.890	0.873
AUC	12-APR	0.998	0.998	0.998	0.994
	9-APR	0.997	0.965	0.996	0.996
	Manual	0.994	0.997	0.988	0.998

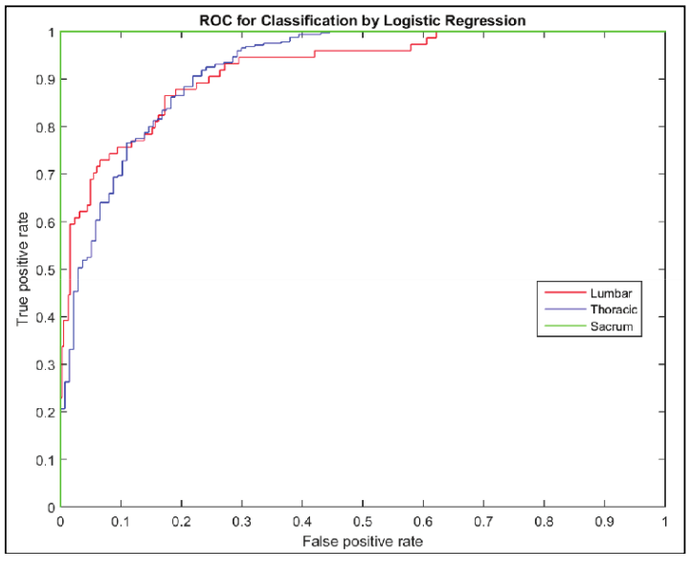

FIGURE 6. ROC plots of sacrum, lumbar, and thoracic bones

CBIRS DESIGN

Figure 7 shows a graphical user interface (GUI) of the developed CBIRS design, consisting of three parts, i.e. 1. query, 2. results, and 3. image information panels. The query panel is the most important part of CBIRS, and it is where all main functions such as image enhancement and segmentation, feature extraction and selection, and retrieval process are handled. Figure 8 presents the labeled query panel, and its nine functions are listed as follows:

1. Browsing images from the image database or folder;
2. Performing image enhancement by using the DWT+HE method;
3. Conducting segmentation by using the 12-APR method;
4. Showing the image that had been browsed, enhanced, or segmented;
5. Resetting to the original image;
6. Selecting the feature extraction technique;
7. Displaying the computed FV;

8. Selecting the distance metric for similarity measurement; and
9. Performing an image retrieval process.

Retrieved images of a query are displayed in the second panel, i.e., the results panel. This panel comprises four main parts, and their functions include the following: the area where the retrieved images are shown, with 20 images per page; -total retrieved images and rank of current images; total number of pages and current page number; and buttons to control the retrieval results (to move to the next or previous page). The third panel is the image information panel. The user simply needs to click an image from the results panel, and important details of that image are shown. This third panel comprises three parts (Figure 9), which include the following: 1) selected image; 2) important details of the image, including metadata; and 3) distance value, which is denoted by d, between the query and the selected images.

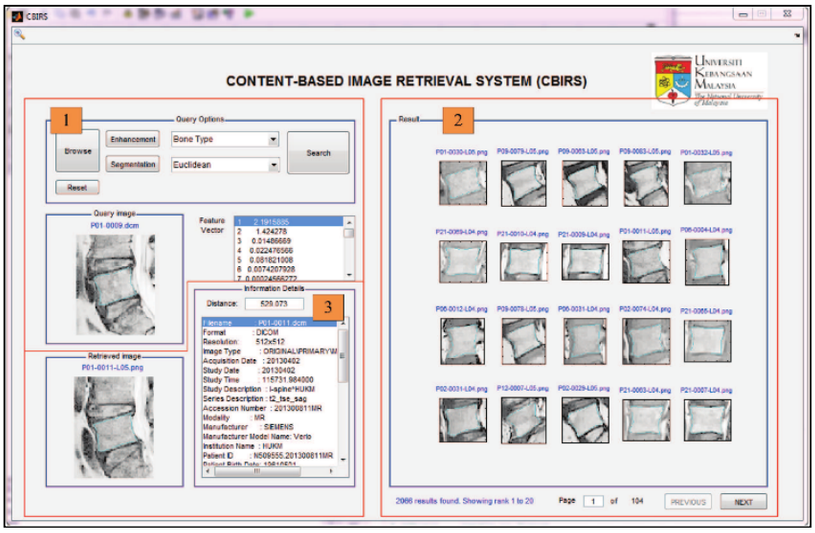

FIGURE 7. User graphical interface of the proposed CBIRS

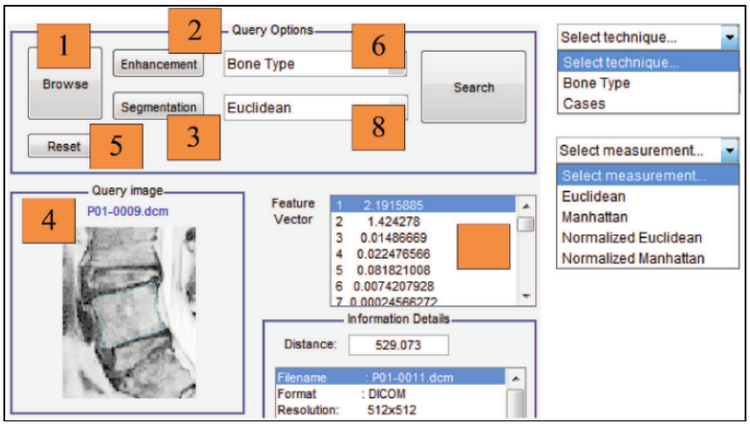

FIGURE 8. Query panel of the proposed CBIRS

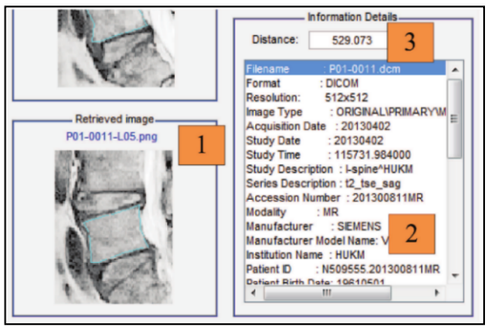

FIGURE 9. Image information panel

FEATURE EXTRACTION AND SELECTION PHASE

The total numbers of shape features extracted using the GSD, Hu, and FD techniques were 15, 7, and 32, respectively. Selected features from each technique were explained in a preliminary work (Ling et al. 2017), in which each extracted feature was analyzed with ANOVA at the significance level of < 0.05. Then, a feature was compared by pairing the bone groups of T, L, and S (i.e., T-L, L-S, and S-T). Our hypothesis is to identify whether the three types of spine vertebra bones have dissimilar features, thus ANOVA can determine if the pairs are statistically and significantly different from one other. Lower significant value will indicate the higher

differences between the pairs. Table 2 shows an example of the significant values for each Hu feature (i.e. Hu has seven features) in ANOVA. The features are evaluated individually and selected in accordance with their ability to differentiate the types of vertebra. Features h3, h5, and h6 obtained significance levels of < 0.05 for all T-L, L-S, and S-T bone pairs. Hence, these features were selected as the optimal features to describe the three vertebral bones for the Hu technique. Then, the same process was applied to GSD and FD. The features that obtained significance levels of < 0.05 for all three bone pairs were selected and combined the four GSD features i.e. and 19 FD features i.e. $f_1, f_2, f_3, f_4, f_6, f_9, f_{11}, f_{13}, f_{14}, f_{17}, f_{18}, f_{22}, f_{23}, f_{25}, f_{26}, f_{27}, f_{28}, f_{31}, f_{32}$. Subsequently, the FV of the global Hu-F descriptor, as derived in Equation (7) was obtained. This FV was then used in the retrieval phase to obtain similar vertebral bone images. Then, the performance and efficiency of the CBIRS system were evaluated on the basis of the precision and recall rates.

TABLE 2. An example of ANOVA results for Hu features

	T-L	L-S	S-T
h1	0.000	0.254	0.000
h2	0.045	0.897	0.074
h3	0.024	0.000	0.000
h4	0.000	0.000	0.058
h5	0.000	0.000	0.000
h6	0.000	0.000	0.000
h7	0.000	0.073	0.002

$$GlobalHu - F = \left[\begin{matrix} G_A, G_{Cy}, G_{Bby}, G_{Eq}, h_3, h_5, h_6, f_1, f_2, f_3, f_4, f_6, f_9, \\ f_{11}, f_{13}, f_{14}, f_{17}, f_{18}, f_{22}, f_{23}, f_{25}, f_{26}, f_{27}, f_{28}, f_{31}, f_{32} \end{matrix} \right] \quad (7)$$

RETRIEVAL PHASE

A total of 2066 MRI images of the human spine in sagittal view, which include 343, 1534, and 189 images of the T, L, and S, respectively, were stored in the database and used in this experiment. In addition, 60 X-ray images comprising five body parts (abdomen, chest, knee, hip, and ankle) were added to diversify the database images. One hundred images for each T, L and S bones were used as query images to test retrieval performance. The performance results portrayed whether the proposed CBIR algorithms could find the correct target, i.e. the results of the lumbar query image must only be L bones. Table 3 shows the average precision rates obtained by all tested thoracic, lumbar, and sacrum images using four different types of distance metrics. The Manhattan metric generally provides the best measurement for thoracic images (0.691), while the normalized Manhattan metric performed well for the lumbar (0.911) and sacrum (0.878) images.

As shown by the P-R graph in Figure 10, the lumbar images are best observed when steady lines are produced for all distance metrics. Thus, visually similar L bones in all 100 test images were retrieved. However, the thoracic images were represented by a decreasing line attributed to some similar lumbar-like shapes in the thoracic class. A precision rate of 0.691 was regarded considerably good, particularly because the thoracic images constituted only 16.7% of the entire spine MRI database. In this study, similar to the thoracic images, the sacrum images were also represented by a somewhat decreasing line pattern at the end of the P-R graph attributed to the insufficient number of images (189) in the database. However, its precision was remarkably high (0.878) considering that the sacrum images were only 9% of the entire MRI database. Figure 11 presents an example of visual retrieval results of the top 20 retrieved images that portray good retrieval and relevant for the lumbar case. Moreover, 19 of 20 images were relevant for the thoracic and sacrum cases.

TABLE 3. Average precision rate for all thoracic, lumbar, and sacrum test images

Distance metric	Thoracic (T)	Lumbar (L)	Sacrum (S)
E	0.632	0.865	0.310
M	0.691	0.874	0.358
NE	0.400	0.906	0.837
NM	0.446	0.911	0.878

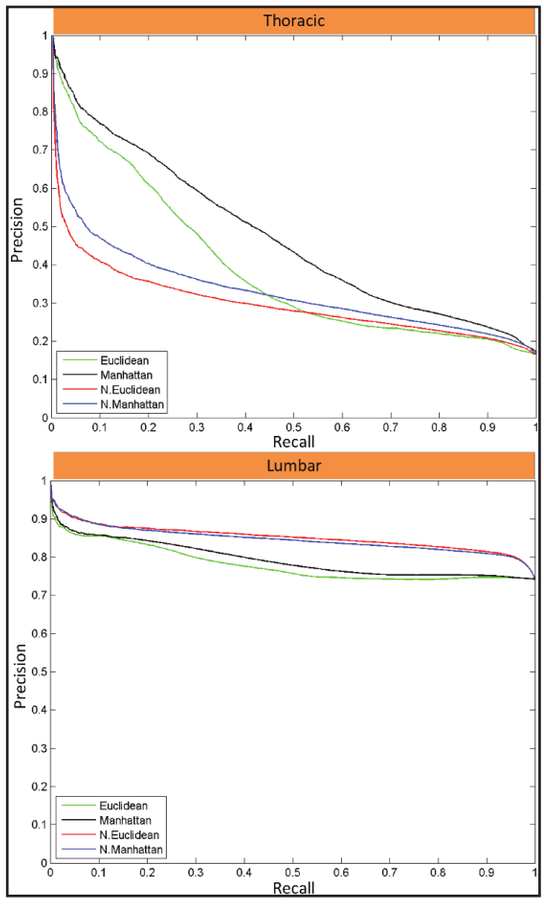

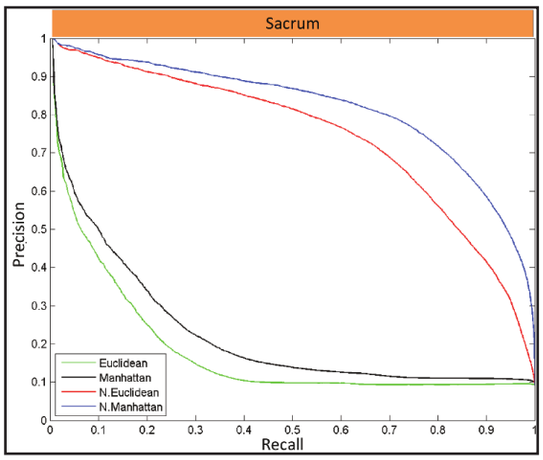

FIGURE 10. Precision-recall graphs of thoracic, lumbar, and sacrum retrieval

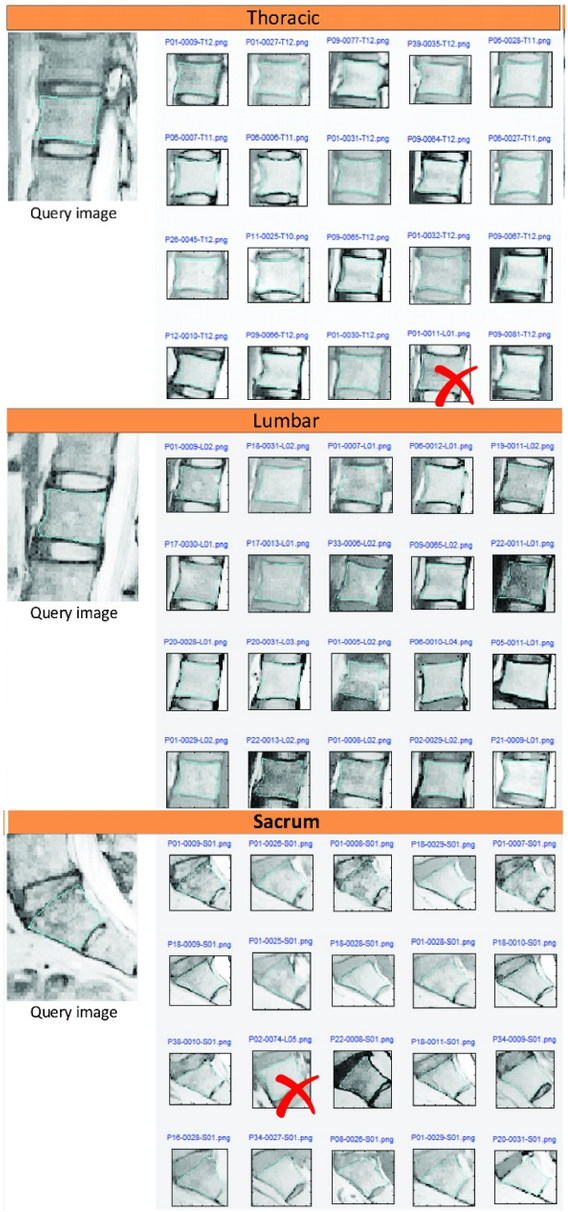

FIGURE 11. An example of visual retrieval results for the first 20 retrieved images using NM distance metric

CONCLUSION

This study presents a new 12-APR method based on ASM for the segmentation of three vertebral bones, namely, T, L and S bones. The proposed method is currently semi-supervised, in which 12 points must be annotated manually on the basis of certain rules. The proposed 12 APR method has successfully segmented the three types of vertebrata. This promising method can be further improved by incorporating an intelligent approach to replace human intervention. Following the segmentation method, the novel global Hu-F feature is derived on the basis of the combinations of GSD, Hu, and FD. The feature is selected according to statistically and significantly different features, as depicted by the ANOVA results. The features are then used to describe the vertebral bones for retrieval purposes. With a total of 2066 MRI images in the database, the CBIRS can effectively retrieve all bone classes given the average precision of 0.691, 0.878, and 0.911 for thoracic, sacral, and lumbar images, respectively. We are looking forward to experimenting our algorithms with additional images and improved segmentation method so that a fully automated retrieval system for MRI spine images can be realized.

ACKNOWLEDGMENT

This research is supported by Dana Impak Perdana (DIP-2018-020) from Universiti Kebangsaan Malaysia.

DECLARATION OF COMPETING INTEREST

None

REFERENCES

Ahmad, W. S. H. M. W., Zaki, W. M. D. W., Hussain, A., Ling, C. S. & Wong, E. Y. H. 2018. Content-Based Image Retrieval for Medical Applications [Publication in Malay]. *J. Kejuruter.* 30(1): 131–143.

Ahmad, W. S. H. M. W. & Fauzi, M. F. A. 2008. Comparison of different feature extraction techniques in content-based image retrieval for CT brain images. *Proceedings of the 2008 IEEE 10th Workshop on Multimedia Signal Processing, MMSP 2008* 503–508. doi:10.1109/MMSP.2008.4665130

Barbieri, P. D., Pedrosa, G. V., Traina, A. J. M. & Nogueira-Barbosa, M. H. 2015. Vertebral body segmentation of spine MR images using superpixels. *Proceedings - IEEE Symposium on Computer-Based Medical Systems* 2015-July: 44–49. doi:10.1109/CBMS.2015.11

Bazila & Mir, A. H. 2014. Intervertebral Discs from Spine MR Images (November): 85–91.

Ben Ayed, I., Punithakumar, K., Minhas, R., Joshi, R. & Garvin, G. J. 2012. Vertebral body segmentation in MRI via convex relaxation and distribution matching. *International Conference on Medical Image Computing and Computer-Assisted Intervention*, hlm. 520–527.

Brisson, P. M. (n.d.). Back Pain Conditons. https://www.nyspinecare.com/back-pain-conditons/ [3 September 2019].

Cootes, T. F., Taylor, C. J., Cooper, D. H. & Graham, J. 1995. Active shape models-their training and applicattion. *Computer Vision and Image Understanding*.

Deng, W. Q., Li, X. M., Gao, X. & Zhang, C. M. 2016. A Modified Fuzzy C-Means Algorithm for Brain MR Image Segmentation and Bias Field Correction. *Journal of Computer Science and Technology* 31(3): 501–511. doi:10.1007/s11390-016-1643-5

Duan, G., Zhao, X., Chen, A. & Liu, Y. Q. 2014. An improved hu moment invariants based classfication method for watermarking algorithm. *IET Conference Publications* 2014(CP657). doi:10.1049/cp.2014.1287

Egger, J., Kapur, T., Dukatz, T., Kolodziej, M., Zukić, D., Freisleben, B. & Nimsky, C. 2012. Square-cut: A segmentation algorithm on the basis of a rectangle shape. *PLoS ONE* 7(2): 1–13. doi:10.1371/journal.pone.0031064

El-Rewaidy, H., Nezafat, M., Jang, J., Nakamori, S., Fahmy, A. S. & Nezafat, R. 2018. Nonrigid active shape model–based registration framework for motion correction of cardiac T1 mapping. *Magnetic Resonance in Medicine* 80(2): 780–791. doi:10.1002/mrm.27068

Gang, Z., Zong-min, M., Lian-qiang, N. & Chun-ming, Z. 2012. Modified Fourier descriptor for shape feature extraction. *J. Cent. South Univ* 19: 488–495. doi:10.1007/s11771

Grierson, M. J., Speckman, R. A., Harrast, M. A. & Herring, S. A. 2015. Stress Fractures of the Lumbar Spine. Dlm. Miller (pnyt.) & Kaeding (pnyt.). *Stress Fractures in Athletes: Diagnosis and Management*, hlm. 83–99. Eds. Cham: Springer International Publishing.

Groen, F. R. J., Delawi, D., Kruyt, M. C. & Oner, F. C. 2016. Extension type fracture of the ankylotic thoracic spine with gross displacement causing esophageal rupture. *European Spine Journal* 25: 183–187. doi:10.1007/s00586-015-4315-1

Gupta, A. (n.d.). The Spine Clinic. http://www.spineclinickanpur.com/. [5 February 2018].

Hille, G., Glaßer, S. & Tönnies, K. 2016. Hybrid Level-Sets for Vertebral Body Segmentation in Clinical Spine MRI. *Procedia Computer Science* 90(July): 22–27. doi:10.1016/j.procs.2016.07.005

Hu, Y. & Li, Z. 2013. An improved shape signature for shape representation and image retrieval. *Journal of Software* 8(11): 2925–2929. doi:10.4304/jsw.8.11.2925-2929

Huang, S. H., Chu, Y. H., Lai, S. H. & Novak, C. L. 2009. Learning-Based Vertebra Detection and Iterative Normalized-Cut Segmentation for Spinal MRI. *IEEE Transactions on Medical Imaging* 28(10): 1595–1605. doi:10.1109/TMI.2009.2023362

Iqbal, K., Odetayo, M. O. & James, A. 2012. Content-based image retrieval approach for biometric security using colour, texture and shape features controlled by fuzzy heuristics. *Journal of Computer and System Sciences* 78(4): 1258–1277. doi:10.1016/j.jcss.2011.10.013

Kadoury, S., Labelle, H. & Paragios, N. 2013. Spine segmentation in medical images using manifold embeddings and higher-order MRFs. *IEEE transactions on medical imaging* 32(7): 1227–1238. doi:10.1109/TMI.2013.2244903

Kaufman, R. P., Ching, R. P., Willis, M. M., Mack, C. D., Gross, J. A. & Bulger, E. M. 2013. Burst fractures of the lumbar spine in frontal crashes. *Accident Analysis and Prevention* 59: 153–163. doi:10.1016/j.aap.2013.05.023

Korhonen, N., Kannus, P., Niemi, S., Parkkari, J. & Sievänen, H. 2014. Rapid increase in fall-induced cervical spine injuries among older Finnish adults between 1970 and 2011. *Age and Ageing* 43(4): 567–571. doi:10.1093/ageing/afu060

Lande, M. V., Bhanodiya, P. & Jain, P. 2014. An effective content-based image retrieval using color, texture and shape feature. *Intelligent Computing, Networking, and Informatics. Springer, New Delhi* 1163–1170. doi:10.1007/978-81-322-1665-0

Ling, C. S., Zaki, W. M. D. W., Hussain, A. & Hamid, H. A. 2017. Semi-automated vertebral segmentation of human spine in MRI images. *2016 International Conference on Advances in Electrical, Electronic and Systems Engineering, ICAEES 2016* 120–124.

Lootus, M., Kadir, T. & Zisserman, A. 2014. Vertebrae detection and labelling in lumbar MR images. *Lect. Notes Comput. Vis. Biomech.* 17: 219–230.

Majkowska, L., Waliłko, E., Molęda, P. & Bohatyrewicz, A. 2014. Thoracic spine fracture in the course of severe nocturnal hypoglycemia in young patients with type 1 diabetes mellitus - The role of low bone mineral density. *American Journal of Emergency Medicine* 32(7): 816.e5-816.e7. doi:10.1016/j.ajem.2013.12.055

Mary Helta Daisy, M., Tamilselvi, S. & Ginu Mol, J. S. 2013. Combined texture and shape features for content based image retrieval. *Proceedings of IEEE International Conference on Circuit, Power and Computing Technologies, ICCPCT 2013* 912–916. doi:10.1109/ICCPCT.2013.6528956

Ming-Kuei, H. 1962. Visual pattern recognition by moment invariants. *IRE Transactions on Information Theory* 66–70.

MRI - Mayo Clinic. (n.d.). https://www.mayoclinic.org/tests-procedures/mri/about/pac-20384768 [25 May 2021].

Mustapha, A., Hussain, A., Samad, S. A., Zulkifley, M. A., Zaki, W. M. D. W. & Hamid, H. A. 2015. Design and development of a content-based medical image retrieval system for spine vertebrae irregularity. *BioMedical Engineering Online* 14(1): 1–24. doi:10.1186/1475-925X-14-6

Neubert, A., Fripp, J., Shen, K., Salvado, O., Schwarz, R., Lauer, L., Engstrom, C., et al. 2011. Automated 3D segmentation of vertebral bodies and intervertebral discs from MRI. *Proceedings - 2011 International Conference on Digital Image Computing: Techniques and Applications, DICTA 2011* 19–24. doi:10.1109/DICTA.2011.12

Pianykh, O. S. 2008. Digital imaging and communications in medicine (DICOM): A practical introduction and survival guide. Springer-Verlag.

Rak, M. & Tönnies, K. D. 2016. On computerized methods for spine analysis in MRI: a systematic review. *International Journal of Computer Assisted Radiology and Surgery* 11(8): 1445–1465. doi:10.1007/s11548-016-1350-2

Rui, Y., She, A. C. & Huang, T. S. 1998. A Modified Fourier Descriptor for Shape Matching in MARS (94): 165–177. doi:10.1142/9789812797988_0014

Schwarzenberg, R., Freisleben, B., Nimsky, C. & Egger, J. 2014. Cube-cut: Vertebral body segmentation in MRI-data through cubic-shaped divergences. *PLoS ONE* 9(4). doi:10.1371/journal.pone.0093389

Sharma, R., Singh, J. & Kaleka, J. S. 2012. Different Approaches of CBIR Techniques. *Int. J. Comput. Distrib. Syst* 1(2): 76–78. Retrieved from www.cirworld.com

Shi, R., Sun, D., Qiu, Z. & Weiss, K. L. 2007. An efficient method for segmentation of MRI spine images. *2007 IEEE/ICME International Conference on Complex Medical Engineering, CME 2007* 713–717. doi:10.1109/ICCME.2007.4381830

Shrinivasacharya, P. & Sudhamani, M. V. 2014. Content based image retrieval system using texture and modified block truncation coding. *ICACCS 2013 - Proceedings of the 2013 International Conference on Advanced Computing and Communication Systems: Bringing to the Table, Futuristic Technologies from Around the Globe*. doi:10.1109/ICACCS.2013.6938770

Syam, B., Victor, J. S. R. & Rao, Y. S. 2013. Efficient similarity measure via genetic algorithm for content based medical image retrieval with extensive features. *Proceedings - 2013 IEEE International Multi Conference on Automation, Computing, Control, Communication and Compressed Sensing, iMac4s 2013* 704–711. doi:10.1109/iMac4s.2013.6526499

Thomas, A. & Sreekumar, K. 2014. A survey on image feature descriptors-color shape and texture. *Int. J. Comput. Sci. Inf. Technol.* 5(6): 7847–7850.

Tong, J., Zhou, R., Liu, S. & Zhu, Q. 2016. Management of fracture and lateral dislocation of the thoracic spine without any neurological deficits: three case reports and review of the literature. *Irish Journal of Medical Science* 185(4): 949–954. doi:10.1007/s11845-014-1237-6

W.S.H.M.W. Ahmad, W.M.D.W. Zaki, M.F.A. Fauzi, & T.W. Haw 2014. Content-based medical image retrieval system for infections and fluids in chest radiographs. *Lecture Notes in Computer Science (including subseries Lecture Notes in Arti icial Intelligence and Lecture Notes in Bioinformatics)* 8870: 14–23. doi:10.1007/978-3-319-12844-3_2

Wang, X. Y., Yu, Y. J. & Yang, H. Y. 2011. An effective image retrieval scheme using color, texture and shape features. *Computer Standards and Interfaces* 33(1): 59–68. doi:10.1016/j.csi.2010.03.004

Wu, Z., Guo, Y., Park, S. H., Gao, Y., Dong, P., Lee, S. W. & Shen, D. 2018. Robust brain ROI segmentation by deformation regression and deformable shape model. *Medical Image Analysis* 43: 198–213. doi:10.1016/j.media.2017.11.001

Wysham, K. D., Murray, S. G., Hills, N., Yelin, E. & Gensler, L. S. 2017. Cervical Spinal Fracture and Other Diagnoses Associated With Mortality in Hospitalized Ankylosing Spondylitis Patients. *Arthritis Care and Research* 69(2): 271–277. doi:10.1002/acr.22934

Yasmin, M., Mohsin, S., Irum, I. & Shari, M. 2013. Content based image retrieval by shape, color and relevance feedback. *Life Science Journal* 10: 593–598.

Zhang, Y., Wang, S., Sun, P. & Phillips, P. 2015. Pathological brain detection based on wavelet entropy and Hu moment invariants. *Bio-Medical Materials and Engineering* 26: S1283–S1290. doi:10.3233/BME-151426

Zhao, F. & Xie, X. 2013. An Overview of Interactive Medical Image Segmentation. *Annals of the British Machine Vision Association* 2013(7): 1–22.

Zhao, Y.-J., Shi, L., Li, J.-C., Griffith, J. F., Ahuja, A. T. & Heng, P. A. 2011. Vertebra segmentation of spine MRI with improved GVF snake based on shape knowledge. *Proceedings of the 2011 International Conference on Machine Learning and Cybernetics* 9: 10–13.

Zukić, D., Vlasák, A., Dukatz, T., Egger, J., Hořínek, D., Nimsky, C. & Kolb, A. 2012. Segmentation of vertebral bodies in MR images. *VMV 2012 - Vision, Modeling and Visualization* 135–142. doi:10.2312/PE/VMV/VMV12/135-142